Journal of Organometallic Chemistry, 459 (1993) 293–301

JOM 23862

Reactions of the hexaruthenium cluster anions $[Ru_6C(CO)_{16}]^{2-}$ and $[Ru_6(CO)_{18}]^{2-}$ with $Au_2\{Ph_2PCH_2PPh_2\}Cl_2$: crystal and molecular structures of $Ru_6C(CO)_{16}Au_2\{Ph_2PCH_2PPh_2\}$ and $Ru_5(CO)_{15}Au_2\{Ph_2PCH_2PPh_2\}$ *

Philip J. Bailey, Michael A. Beswick, Jack Lewis, Paul R. Raithby and M. Carmen Ramirez de Arellano

University Chemical Laboratory, Lensfield Road, Cambridge CB2 1EW (UK)

(Received May 24, 1993)

Abstract

The reaction of the carbido dianion $[Ru_6C(CO)_{16}]^{2-}$ with $Au_2\{Ph_2PCH_2PPh_2\}Cl_2$, in dichloromethane, in the presence of $TlPF_6$, affords the neutral cluster $Ru_6C(CO)_{16}Au_2\{Ph_2PCH_2PPh_2\}$ (**1**) in 90% yield. An X-ray analysis of **1** shows that the octahedral ruthenium core has remained intact, and that the two Au atoms of the chelating gold phosphine bridge two adjacent edges of one of the triangular faces of the Ru_6 octahedron. In marked contrast, the reaction of the non-carbido dianion $[Ru_6(CO)_{18}]^{2-}$ with $Au_2\{Ph_2PCH_2PPh_2\}Cl_2$ under similar reaction conditions leads to the breakdown of the octahedral ruthenium core and the formation of $Ru_5(CO)_{15}Au_2\{Ph_2PCH_2PPh_2\}$ (**2**) in *ca.* 50% yield. The X-ray analysis of **2** shows that the ruthenium atoms adopt a trigonal bipyramidal framework with the Au atoms of the $Au_2\{Ph_2PCH_2PPh_2\}$ ligand μ_3-capping adjacent faces of the trigonal bipyramid in a manner not previously observed for mixed ruthenium–gold clusters.

1. Introduction

Heteronuclear clusters which contain one or more Group 11 metals remain an important area of cluster research. The presence of Group 11 metals introduces a polarity into the metal framework and generates metal geometries that are not observed in homometal clusters [1]. In clusters which contain more than one Group 11 metal, examples are known where two Group 11 metals are within bonding distance of each other and there are also examples where the two Group 11 metals are well separated [1]. The use of chelating digold phosphine cations such as $[Au_2\{Ph_2PCH_2PPh_2\}]^{2+}$, $[Au_2\{Ph_2PCH_2CH_2PPh_2\}]^{2+}$ and $[Au_2\{Ph_2PC{\equiv}CPPh_2\}]^{2+}$ forces the two Au atoms to remain in relatively close contact in the final product. Despite this, a number of different modes of coordination of the bidentate gold-containing ligands have been observed in a range of tri- and tetranuclear ruthenium and osmium cluster systems [2–4]. We have recently extended the synthetic method to higher nuclearity cluster anions of ruthenium and have obtained the pentaruthenium cluster $Ru_5C(CO)_{14}Au_2\{Ph_2PCH_2CH_2PPh_2\}$ [5]. With the increase in nuclearity comes a higher probability of finding a greater variety of coordination modes for the gold-containing phosphine ligands. We have also developed better, high yield routes to the hexaruthenium cluster anions $[Ru_6C(CO)_{16}]^{2-}$ and $[Ru_6(CO)_{18}]^{2-}$ and this has allowed us to carry out the reactions of these anions with $[Au_2\{Ph_2PCH_2PPh_2\}]^{2+}$. We now report the more efficient routes to the hexaruthenium anions and the results of the reactions of these species with the bidentate gold-containing cation. The products formed emphasize the marked difference in reactivity between the carbido and non-carbido hexanuclear clusters. It is well known that carbido-clusters are less likely to undergo fragmentation reactions than the related non-carbido clusters because the central carbon atom helps to hold the

Correspondence to: Professor the Lord Lewis.

* Dedicated to Professor E.O. Fischer on the occasion of his 75th birthday.

0022-328X/93/$6.00

© 1993 – Elsevier Sequoia S.A. All rights reserved

metal framework together [6]. In this case, the reaction of $[Ru_6C(CO)_{16}]^{2-}$ with $[Au_2\{Ph_2PCH_2PPh_2\}]^{2+}$ affords the hexaruthenium cluster $Ru_6C(CO)_{16}Au_2\{Ph_2PCH_2PPh_2\}$ whereas the reaction of $[Ru_6(CO)_{18}]^{2-}$ with $Au_2\{Ph_2PCH_2PPh_2\}]^{2+}$ leads to cluster breakdown and the formation of the pentaruthenium cluster $Ru_5(CO)_{15}Au_2\{Ph_2PCH_2PPh_2\}$.

2. Results and discussion

Recent studies on the pyrolysis and thermolysis of derivatives of $Ru_3(CO)_{12}$ have led to the high yield synthesis of the cluster anions $[Ru_6C(CO)_{16}]^{2-}$ and $[Ru_6(CO)_{18}]^{2-}$. The new method avoids the use of sodium which is a feature of the established preparation method [7]. The anion $[Ru_6C(CO)_{16}]^{2-}$ is obtained as the $[N(PPh_3)_2]^+$ salt, in *ca.* 50% yield, together with $[Ru_{10}C_2(CO)_{24}]^{2-}$ (*ca.* 20% yield) from the pyrolysis of $Ru_3H(CO)_{10}(C_5H_4N)$, at 150°C for 48 h. The pyridine derivative is itself obtained from $Ru_3(CO)_{12}$ *via* the reaction of the bis-acetonitrile derivative with pyridine. The dianion $[Ru_6(CO)_{18}]^{2-}$ is obtained as the $[N(PPh_3)]^+$ salt, in *ca.* 60% yield, from the thermolysis of $Ru_3(CO)_{12}$, in acetonitrile for 3 h, followed by the addition of excess $[N(PPh_3)_2]BF_4$ and separation of the mixture by TLC using 1:1 acetone/hexane as eluent. These convenient synthetic routes to the hexaruthenium anions has allowed their reactions with a range of cationic species to be studied.

The reaction of the carbido dianion $[Ru_6C(CO)_{16}]^{2-}$ with 1.1 equiv. of $Au_2\{Ph_2PCH_2PPh_2\}Cl_2$, in the presence of excess $TlPF_6$, which acts as a halide abstractor, in CH_2Cl_2, affords, after work-up, a red mixed-metal cluster **1** in 80–90% yield. This complex was initially characterized as $Ru_6C(CO)_{16}Au_2\{Ph_2PCH_2PPh_2\}$ (**1**) from spectroscopic data (Table 1), and the assignment confirmed by a single-crystal X-ray analysis.

The molecular structure of $Ru_6C(CO)_{16}Au_2\{Ph_2PCH_2PPh_2\}$ (**1**) is shown in Fig. 1 while selected bond

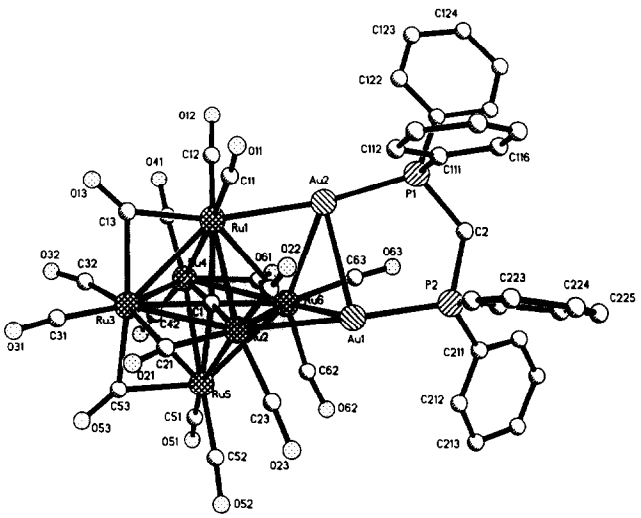

Fig. 1. The molecular structure of $Ru_6C(CO)_{16}Au_2\{Ph_2PCH_2PPh_2\}$ (**1**) showing the atom numbering scheme. Hydrogen atoms have been omitted for clarity.

parameters are listed in Table 2. The central octahedral Ru_6 core geometry with the interstitial carbide observed in the parent dianion $[Ru_6C(CO)_{16}]^{2-}$ [8] is retained in the structure of **1**. Four of the coordinated carbonyl ligands are edge bridging and the remaining twelve are terminal. This ligand arrangement is similar to that found in the $[Ph_4As]^+$ salt of the parent dianion [8]. The two Au atoms of the chelating $Au_2\{Ph_2PCH_2PPh_2\}$ ligand bridge adjacent edges of the Ru_6 octahedron in what may be described as a $\mu_2:\mu_2$ mode. There is also a relatively short Au–Au contact, and the metal framework as a whole may be described as a Ru_6 octahedron fused with a Ru_3Au_2 square-based pyramid. The $\mu_2:\mu_2$ coordination mode has previously been observed in the structures of $Ru_4H_2(CO)_{12}Au_2\{Ph_2PCH_2CH_2PPh_2\}$ [9] and $Ru_4H_2(CO)_{12}Au_2\{Ph_2AsCH_2PPh_2\}$ [2]. This contrasts the structure of $Ru_6C(CO)_{16}Au_2(PMePh_2)_2$ [10] where although the two Au atoms adopt μ_2 bonding modes there is no short contact between the Au atoms. A third bonding

TABLE 1. Spectroscopic data for complexes **1** and **2**

Compound	IR (hexane) ν(CO) (cm^{-1})	MS *m/e* (−ve FAB)	$^{31}P\{^1H\}$ NMR (CD_2Cl_2)	^1H NMR (CD_2Cl_2)
1	2068m, 2026s 1980m, 1838w, br	1845 (calc. 1848)	−90.78s	3.87 (t, 2H) 7.3–7.6 (m, 20H)
2	2074s, 2046s 2024s, 2006s 1984w, 1920w	1676 corresponds to $M^+ - CO$ (calc. 1704)	−97.8s	3.56 (t, 2H) 7.3–7.4 (m, 20H)

TABLE 2. Selected bond distances (Å) and angles (°) for $Ru_6C(CO)_{16}Au_2\{Ph_2PCH_2PPh_2\}$ (1)

Ru(1)–Au(2)	2.687(2)	Ru(1)–Ru(3)	2.827(2)
Ru(1)–Ru(2)	2.881(2)	Ru(1)–Ru(4)	2.927(2)
Ru(1)–Ru(6)	3.093(2)	Ru(2)–Au(1)	2.743(2)
Ru(2)–Ru(5)	2.885(2)	Ru(2)–Ru(3)	2.939(2)
Ru(2)–Ru(6)	3.117(2)	Ru(3)–Ru(5)	2.821(2)
Ru(3)–Ru(4)	2.843(2)	Ru(4)–Ru(6)	2.785(2)
Ru(4)–Ru(5)	2.915(2)	Ru(5)–Ru(6)	2.898(2)
Ru(6)–Au(1)	2.815(2)	Ru(6)–Au(2)	2.951(2)
Au(1)–Au(2)	2.863(1)	Au(1)–P(2)	2.311(5)
Au(2)–P(1)	2.309(5)		
Au(2)–Ru(1)–Ru(3)	143.97(6)	Au(2)–Ru(1)–Ru(2)	85.95(5)
Ru(3)–Ru(1)–Ru(2)	61.96(5)	Au(2)–Ru(1)–Ru(4)	108.77(6)
Ru(3)–Ru(1)–Ru(4)	59.18(5)	Ru(2)–Ru(1)–Ru(4)	90.47(6)
Au(2)–Ru(1)–Ru(6)	60.93(5)	Ru(3)–Ru(1)–Ru(6)	88.37(6)
Ru(2)–Ru(1)–Ru(6)	62.78(5)	Ru(4)–Ru(1)–Ru(6)	55.02(5)
Au(1)–Ru(2)–Ru(1)	92.84(6)	Au(1)–Ru(2)–Ru(5)	102.37(6)
Ru(1)–Ru(2)–Ru(5)	90.11(6)	Au(1)–Ru(2)–Ru(3)	141.80(6)
Ru(1)–Ru(2)–Ru(3)	58.10(5)	Ru(5)–Ru(2)–Ru(3)	57.94(5)
Au(1)–Ru(2)–Ru(6)	56.99(4)	Ru(1)–Ru(2)–Ru(6)	61.94(5)
Ru(5)–Ru(2)–Ru(6)	57.59(5)	Ru(3)–Ru(2)–Ru(6)	85.96(5)
Ru(5)–Ru(3)–Ru(1)	92.55(6)	Ru(5)–Ru(3)–Ru(4)	61.95(6)
Ru(1)–Ru(3)–Ru(4)	62.18(5)	Ru(5)–Ru(3)–Ru(2)	60.09(5)
Ru(1)–Ru(3)–Ru(2)	59.93(5)	Ru(4)–Ru(3)–Ru(2)	91.01(6)
Ru(6)–Ru(4)–Ru(3)	94.42(6)	Ru(6)–Ru(4)–Ru(5)	61.08(5)
Ru(3)–Ru(4)–Ru(5)	58.66(5)	Ru(6)–Ru(4)–Ru(1)	65.51(5)
Ru(3)–Ru(4)–Ru(1)	58.64(5)	Ru(5)–Ru(4)–Ru(1)	88.63(6)
Ru(3)–Ru(5)–Ru(2)	61.97(5)	Ru(3)–Ru(5)–Ru(6)	92.45(6)
Ru(2)–Ru(5)–Ru(6)	92.45(6)	Ru(2)–Ru(5)–Ru(6)	65.22(5)
Ru(3)–Ru(5)–Ru(4)	59.39(5)	Ru(2)–Ru(5)–Ru(4)	90.64(6)
Ru(6)–Ru(5)–Ru(4)	57.25(5)	Ru(4)–Ru(6)–Au(1)	141.48(7)
Ru(4)–Ru(6)–Ru(5)	61.68(5)	Au(1)–Ru(6)–Ru(5)	100.30(6)
Ru(4)–Ru(6)–Au(2)	105.48(6)	Au(1)–Ru(6)–Au(2)	59.48(4)
Ru(5)–Ru(6)–Au(2)	131.83(6)	Ru(4)–Ru(6)–Au(1)	59.46(5)
Au(1)–Ru(6)–Ru(1)	87.10(5)	Ru(5)–Ru(6)–Ru(1)	85.81(6)
Au(2)–Ru(6)–Ru(1)	52.73(4)	Ru(4)–Ru(6)–Ru(2)	88.48(6)
Au(1)–Ru(6)–Ru(2)	54.80(4)	Ru(5)–Ru(6)–Ru(2)	57.19(5)
Au(2)–Ru(6)–Au(2)	77.45(5)	Ru(1)–Ru(6)–Ru(2)	55.29(5)
P(2)–Au(1)–Ru(2)	169.54(13)	P(2)–Au(1)–Ru(6)	121.17(13)
Ru(2)–Au(1)–Ru(6)	68.21(5)	P(2)–Au(1)–Au(2)	95.08(12)
Ru(2)–Au(1)–Au(2)	85.29(4)	Ru(6)–Au(1)–Au(2)	62.63(4)
P(1)–Au(2)–Ru(1)	164.64(13)	P(1)–Au(2)–Au(1)	89.31(11)
Ru(1)–Au(2)–Au(1)	94.45(4)	P(1)–Au(2)–Ru(6)	127.46(12)
Ru(1)–Au(2)–Ru(6)	66.34(5)	Au(1)–Au(2)–Ru(6)	57.89(4)

mode, $\mu_3:\mu_2$, in which one Au atom caps a metal triangle and the second Au atom bridges one of the capped metal–metal edges and also forms a relatively short Au–Au contact is also known. This type of structure has been observed in $Ru_5WC(CO)_{17}Au_2(PEt_3)_2$ [10] and $Ru_4H_2(CO)_{12}Au_2(PPh_3)$ [11]. It is clear that the presence of either two monodentate or a chelating digold phosphine ligand has a drastic effect on the resultant metal framework geometry. It seems likely that the steric constraints of the chelating phosphine forces the $\mu_2:\mu_2$ geometry on the two Au atoms in the structure of **1** coupled with the need to retain the Au–Au contact.

In terms of electron counting, if each of the Au atoms of the $Au_2\{Ph_2PCH_2PPh_2\}$ group donates one electron to the cluster, then the complex as a whole is an 86 electron system, which is consistent with the octahedral ruthenium core geometry. The two longest Ru–Ru distances in the structure are the two octahedral edges bridged by the two Au atoms (Ru(1)–Ru(6) 3.093(2) and Ru(2)–Ru(6) 3.117(2) Å). The remaining Ru–Ru distances in the structure lie in the range 2.821(2)–2.939(2) Å which is similar to the range of values 2.832(1)–3.001(1) Å found in $[Ru_6C(CO)_{16}]^{2-}$ [8]. The average Ru–C(carbide) distance of 2.06 Å is also similar to that found in the parent dianion. The Ru–Au distances show significant asymmetry, with the two longer distances both involving Ru(6). Overall, the range of Ru–Au distances (2.687(2)–2.951(2) Å) in **1** is similar to that found in $Ru_4H_2(CO)_{12}Au_2\{Ph_2PCH_2PPh_2\}$ (2.682(1)–2.947(2) Å) [12], although the Au–Au separation in **1** is *ca.* 0.04 Å longer than the value of 2.823(1) Å in $Ru_4H_2(CO)_{12}Au_2\{Ph_2PCH_2PPh_2\}$ [12].

The reaction of the non-carbido dianion $[Ru_6(CO)_{18}]^{2-}$ with $Au_2\{Ph_2PCH_2PPh_2\}Cl_2$ was carried out under the same conditions as for $[Ru_6C(CO)_{16}]^{2-}$. In this case, however, the major, red-brown product was formulated as the pentaruthenium cluster $Ru_5(CO)_{15}Au_2\{Ph_2PCH_2PPh_2\}$ (**2**) from spectroscopic data (Table 1), and the assignment confirmed by a single-crystal X-ray analysis.

The molecular structure of $Ru_5(CO)_{15}Au_2\{Ph_2PCH_2PPh_2\}$ (**2**) is shown in Fig. 2 while selected bond lengths and angles are presented in Table 3. The ruthenium framework is best described as a trigonal

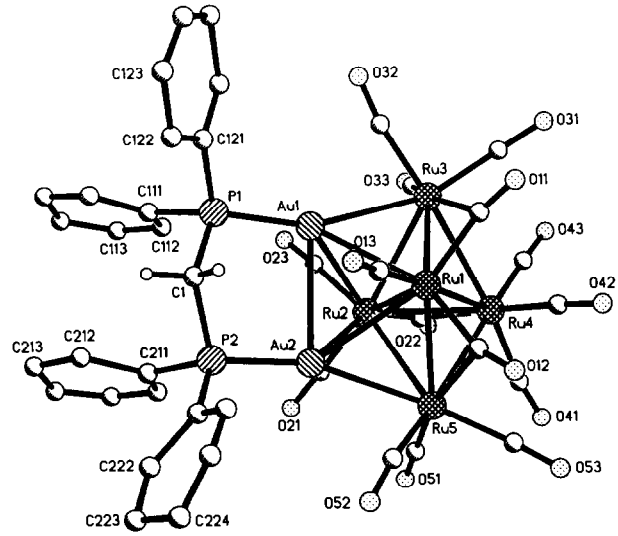

Fig. 2. The molecular structure of $Ru_5(CO)_{15}Au_2\{Ph_2PCH_2PPh_2\}$ (**2**) showing the atom numbering scheme. Hydrogen atoms have been omitted for clarity.

TABLE 3. Selected bond lengths (Å) and angles (°) for $Ru_5(CO)_{15}Au_2\{Ph_2PCH_2PPh_2\}$ (2)

Ru(1)–Ru(2)	3.027(2)	Ru(1)–Ru(3)	2.698(3)
Ru(1)–Ru(4)	2.916(3)	Ru(1)–Ru(5)	2.693(3)
Ru(1)–Au(1)	2.900(3)	Ru(1)–Au(2)	2.946(3)
Ru(2)–Ru(3)	3.005(3)	Ru(2)–Ru(4)	2.792(3)
Ru(2)–Ru(5)	3.051(3)	Ru(2)–Au(1)	2.877(2)
Ru(2)–Au(2)	2.820(3)	Ru(3)–Ru(4)	2.933(3)
Ru(3)–Au(1)	2.829(3)	Ru(4)–Ru(5)	2.919(3)
Ru(5)–Au(2)	2.785(3)	Au(1)–Au(2)	2.944(2)
Au(1)–P(1)	2.312(7)	Au(2)–P(2)	2.306(7)
Ru(2)–Ru(1)–Ru(3)	63.0(1)	Ru(2)–Ru(1)–Ru(4)	56.0(1)
Ru(3)–Ru(1)–Ru(4)	62.9(1)	Ru(2)–Ru(1)–Ru(5)	64.1(1)
Ru(3)–Ru(1)–Ru(5)	118.4(1)	Ru(4)–Ru(1)–Ru(5)	62.6(1)
Ru(2)–Ru(1)–Au(1)	58.0(1)	Ru(3)–Ru(1)–Au(1)	60.6(1)
Ru(4)–Ru(1)–Au(1)	106.1(1)	Ru(5)–Ru(1)–Au(1)	111.9(1)
Ru(2)–Ru(1)–Au(2)	56.3(1)	Ru(3)–Ru(1)–Au(2)	110.5(1)
Ru(4)–Ru(1)–Au(2)	103.4(1)	Ru(5)–Ru(1)–Au(2)	59.0(1)
Au(1)–Ru(1)–Au(2)	60.5(1)	Ru(1)–Ru(2)–Ru(3)	53.1(1)
Ru(1)–Ru(2)–Ru(4)	60.0(1)	Ru(3)–Ru(2)–Ru(4)	60.7(1)
Ru(1)–Ru(2)–Ru(5)	52.6(1)	Ru(3)–Ru(2)–Ru(5)	99.8(1)
Ru(4)–Ru(2)–Ru(5)	59.7(1)	Ru(1)–Ru(2)–Au(1)	58.8(1)
Ru(3)–Ru(2)–Au(1)	57.4(1)	Ru(4)–Ru(2)–Au(1)	110.2(1)
Ru(5)–Ru(2)–Au(1)	102.8(1)	Ru(1)–Ru(2)–Au(2)	60.4(1)
Ru(3)–Ru(2)–Au(2)	105.5(1)	Ru(4)–Ru(2)–Au(2)	110.1(1)
Ru(5)–Ru(2)–Au(2)	56.5(1)	Au(1)–Ru(2)–Au(2)	62.2(1)
Ru(1)–Ru(3)–Ru(2)	63.9(1)	Ru(1)–Ru(3)–Ru(4)	62.2(1)
Ru(2)–Ru(3)–Ru(4)	56.1(1)	Ru(1)–Ru(3)–Au(1)	63.2(1)
Ru(2)–Ru(3)–Au(1)	59.0(1)	Ru(4)–Ru(3)–Au(1)	107.6(1)
Ru(1)–Ru(4)–Ru(2)	64.0(1)	Ru(1)–Ru(4)–Ru(3)	54.9(1)
Ru(2)–Ru(4)–Ru(3)	63.3(1)	Ru(1)–Ru(4)–Ru(5)	55.0(1)
Ru(2)–Ru(4)–Ru(5)	64.5(1)	Ru(3)–Ru(4)–Ru(5)	104.7(1)
Ru(1)–Ru(5)–Ru(2)	63.3(1)	Ru(1)–Ru(5)–Ru(4)	62.4(1)
Ru(2)–Ru(5)–Ru(4)	55.7(1)	Ru(1)–Ru(5)–Au(2)	65.0(1)
Ru(2)–Ru(5)–Au(2)	57.6(1)	Ru(4)–Ru(5)–Au(2)	107.5(1)
Ru(1)–Au(1)–Ru(2)	63.2(1)	Ru(1)–Au(1)–Ru(3)	56.2(1)
Ru(2)–Au(1)–Ru(3)	63.5(1)	Ru(1)–Au(1)–Au(2)	60.5(1)
Ru(2)–Au(1)–Au(2)	57.9(1)	Ru(3)–Au(1)–Au(2)	106.9(1)
Ru(1)–Au(1)–P(1)	129.4(2)	Ru(2)–Au(1)–P(1)	138.2(2)
Ru(3)–Au(1)–P(1)	158.1(2)	Au(2)–Au(1)–P(1)	91.7(2)
Ru(1)–Au(2)–Ru(2)	63.3(1)	Ru(1)–Au(2)–Ru(5)	56.0(1)
Ru(2)–Au(2)–Ru(5)	65.9(1)	Ru(1)–Au(2)–Au(1)	59.0(1)
Ru(2)–Au(2)–Au(1)	59.9(1)	Ru(5)–Au(2)–Au(1)	108.0(1)
Ru(1)–Au(2)–P(2)	130.2(2)	Ru(2)–Au(2)–P(2)	138.4(2)
Ru(5)–Au(2)–P(2)	155.5(2)	Au(1)–Au(2)–P(2)	91.9(2)

bipyramid to which are coordinated three bridging and twelve terminal carbonyls. The two Au atoms of the chelating $Au_2\{Ph_2PCH_2PPh_2\}$ ligand coordinate to two adjacent faces of the Ru_5 trigonal bipyramid in a $\mu_3:\mu_3$ bonding mode, while the Au–Au contact is also retained. Overall the Ru_5Au_2 framework may be described as a pentagonal bipyramid with two Ru atoms in the axial sites. The trigonal bipyramidal metal geometry has not been previously structurally characterized for ruthenium although a number of analogous osmium structures have been reported [13]. The $\mu_3:\mu_3$ mode of bonding for two gold phosphine fragments has already been observed in the structures of $Os_4(CO)_{12}(AuPMePh_2)_2$ [14] and $Os_8(CO)_{22}(AuPPh_3)_2$ [15]. However, in both these cases the Au ··· Au separation is over 4 Å and there can be no direct interaction between the two Au atoms. In the structure of **2** the Au–Au separation is 2.944(2) Å, and some form of direct interaction may be contemplated, although the distance is *ca.* 0.08 Å longer than the value found in **1**. The structure of **2** represents the first example of the $\mu_3:\mu_3$ mode of coordination of two Au atoms of a gold phosphine in which a relatively short Au–Au contact is retained. This result is presumably a constraint placed on the structure by the presence of the chelating bidentate $Au_2\{Ph_2PCH_2PPh_2\}$ ligand.

In terms of electron counting, if the $Au_2\{Ph_2PCH_2PPh_2\}$ group acts as a two electron donor, the overall electron count is 72 electrons, which is consistent with the trigonal bipyramidal geometry of the ruthenium

TABLE 4. Crystal data and data collection parameters for **1** and **2**

Compound	**1**	**2**
Formula	$C_{42}H_{22}Au_2O_{16}P_2Ru_6$	$C_{40}H_{22}Au_2O_{15}P_2Ru_5 + 2CH_3OH$
FW	1844.89	1767.9
Colour; habit	black prism	black block
Crystal size (mm)	0.24×0.22×0.20	0.52×0.32×0.26
Crystal system	Monoclinic	Monoclinic
Space group	$P2_1/c$	$P2_1/c$
a (Å)	15.383(3)	17.034(7)
b (Å)	15.865(3)	12.781(5)
c (Å)	20.863(4)	23.092(10)
β (°)	108.03(3)	93.14(3)
V (Å^3)	4842(2)	5020(4)
Z	4	4
Calc. density (g cm^{-3})	2.531	2.339
Absorption coeff. (cm^{-1})	79.87	74.16
$F(000)$	3416	3304
2θ range (°)	5–45	5–45
Scan type	$\omega-2\theta$	$\omega-2\theta$
Scan speed (°/min)	2.93–29.3	3.00–19.5
Scan range (°)	1.4+K$_\alpha$ separation	1.6+K$_\alpha$ separation
Reflections collected	7012	7084
Unique reflections	6516 (R_{int} = 0.027)	6597 (R_{int} = 0.011)
Observed reflections [$F > 4\sigma(F)$]	3992	3970
Transmission factors		
Max.	0.180	0.155
Min.	0.115	0.097
Goodness-of-fit	1.062	1.47
R indices		
R_1	0.049	0.063
wR_2 (all data)	0.108	0.082
Largest diff. peak (e Å^{-3})	2.004	2.08
Largest diff. hole (e Å^{-3})	−0.875	−1.35

TABLE 5. Atomic coordinates ($\times 10^4$) and equivalent isotropic displacement parameters ($Å^2 \times 10^3$); U_{eq} is defined as one-third of the trace of the orthogonalized U_{ij} tensor for **1**

	x	y	z	U_{eq}
Ru(1)	6198.8(10)	2342.6(9)	792.1(7)	29.2(8)
Ru(2)	5660.7(10)	3056.2(8)	1881.9(7)	29.4(9)
Ru(3)	4827.5(10)	1505.2(9)	1190.2(7)	31.4(8)
Ru(4)	6570.8(11)	722.7(9)	1496.2(8)	36.1(9)
Ru(5)	5924.3(11)	1441.9(9)	2551.87(7)	37.4(10)
Ru(6)	7509.5(10)	2083.3(9)	2237.7(7)	31.2(9)
Au(1)	7323.9(5)	3820.2(4)	2438.6(4)	33.5(4)
Au(2)	7693.2(5)	3319.4(5)	1230.3(4)	35.0(4)
C(1)	6149(12)	1894(10)	1701(8)	34(11)
C(11)	5920(13)	3387(13)	299(9)	44(13)
C(12)	6802(13)	1904(14)	206(11)	59(13)
C(13)	4935(13)	1929(10)	199(10)	35(12)
C(21)	4364(14)	2948(12)	1567(11)	55(13)
C(22)	5580(13)	4168(13)	1474(10)	46(13)
C(23)	5683(15)	3480(12)	2726(11)	53(16)
C(31)	3528(14)	1488(13)	830(9)	48(13)
C(32)	4858(14)	394(13)	856(9)	45(15)
C(41)	6908(15)	165(13)	805(11)	60(16)
C(42)	6559(14)	−352(15)	1859(13)	73(13)
C(51)	6289(15)	508(14)	3088(12)	64(15)
C(52)	5562(18)	1874(13)	3271(11)	67(21)
C(53)	4673(12)	933(10)	2092(8)	31(12)
C(61)	7922(13)	936(11)	2044(9)	40(13)
C(62)	7753(15)	1920(12)	3159(10)	52(16)
C(63)	8751(15)	2441(12)	2434(1)	53(14)
O(11)	5731(11)	3970(9)	−33(7)	73(13)
O(12)	7166(11)	1686(12)	−178(8)	98(13)
O(13)	4455(8)	1898(8)	−337(6)	46(8)
O(21)	3609(10)	3142(9)	1438(10)	92(10)
O(22)	5473(10)	4807(9)	1247(8)	65(11)
O(23)	5628(13)	3776(9)	3223(9)	94(18)
O(31)	2750(10)	1480(10)	665(7)	73(9)
O(32)	4669(9)	−253(8)	618(7)	50(9)
O(41)	7136(11)	−148(12)	392(8)	112(12)
O(42)	6606(17)	−1012(10)	2104(12)	141(25)
O(51)	6534(12)	−64(11)	3453(10)	113(14)
O(52)	5322(16)	2093(12)	3701(8)	126(23)
O(53)	4120(10)	533(9)	2221(7)	69(11)
O(61)	8607(10)	502(8)	2179(7)	61(9)
O(62)	8037(11)	1839(11)	3745(7)	88(13)
O(63)	9526(10)	2547(9)	2608(7)	69(10)
P(1)	8743(3)	4400(3)	1389(2)	33(3)
P(2)	8590(3)	4684(3)	2816(2)	33(3)
C(2)	9356(11)	4554(10)	2283(7)	27(12)
C(111)	8275(12)	5427(12)	1136(9)	39(12)
C(112)	7364(14)	5514(12)	751(9)	47(14)
C(113)	7035(15)	6317(15)	551(13)	81(13)
C(114)	7529(16)	7049(15)	730(11)	67(17)
C(115)	8409(17)	6938(13)	1101(10)	64(19)
C(116)	8817(15)	6142(13)	1307(9)	54(15)
C(121)	9630(14)	4222(11)	1007(9)	41(14)
C(122)	9420(12)	3794(13)	426(10)	51(11)
C(123)	10079(19)	3634(14)	98(10)	67(21)
C(124)	10949(17)	3954(14)	375(12)	65(18)
C(125)	11144(15)	4388(15)	940(12)	65(14)
C(126)	10530(16)	4532(13)	1270(10)	65(19)
C(211)	9294(11)	4361(10)	3625(8)	31(11)
C(212)	8901(13)	4060(12)	4083(8)	47(13)
C(213)	9347(15)	3787(15)	4714(11)	70(15)

TABLE 5 *(continued)*

	x	y	z	U_{eq}
C(214)	10319(16)	3812(14)	4938(10)	66(18)
C(215)	10750(16)	4078(13)	4504(9)	63(16)
C(216)	10230(13)	4360(13)	3863(10)	52(13)
C(221)	8440(12)	5809(11)	2849(8)	32(12)
C(222)	7581(13)	6143(12)	2490(10)	49(13)
C(223)	7447(14)	7032(13)	2470(11)	58(13)
C(224)	8149(21)	7515(13)	2861(13)	78(26)
C(225)	8950(18)	7209(13)	3213(11)	60(20)
C(226)	9141(16)	6334(13)	3211(9)	58(16)

core. As observed in the structure of **1**, the longest Ru–Ru edge lengths in **2** are those associated with the capping Au atoms. The Ru(1)–Ru(2), Ru(2)–Ru(3) and Ru(2)–Ru(5) edge lengths lie in the range 3.005(3)–3.051(3) Å, but the other two edge of the capped faces Ru(1)–Ru(3) and Ru(1)–Ru(5) are short, at 2.698(3) and 2.693(3) Å, respectively. Consistent with this, the capping Au atoms show significant asymmetry with shorter Au–Ru contacts to Ru(2) (2.820(3) and 2.877(3) Å) than to Ru(1) (2.900(3) and 2.946(3) Å).

The difference in reactivity between the carbido and non-carbido hexanuclear dianions of ruthenium with the chelating dication $[Au_2\{Ph_2PCH_2PPh_2\}]^{2+}$ reflects the increased stability towards cluster fragmentation in the carbido complex. In the synthesis of **1**, the expected redox condensation reaction occurred to give the Ru_6Au_2 cluster, whereas in the synthesis of **2**, cluster breakdown occurred and the Ru_5Au_2 cluster was obtained as the major product. Clearly, the presence of the chelating digold phosphine has a marked influence on the conformation of the product formed, and the metal core geometry may differ significantly from observed when two monodentate gold phosphine ligands are employed instead.

3. Experimental details

All the reactions were carried out under an atmosphere of dry, oxygen-free nitrogen using standard Schlenk and vacuum line techniques. Technical grade solvents were purified by standard procedures. Mass spectra were recorded on the Kratos model MS 902, IR spectra on a Perkin-Elmer 1710 FT-IR spectrometer and ^1H and ^{31}P NMR spectra on a Bruker WH 250 MHz spectrometer, respectively. $Ru_3(CO)_{12}$ was prepared by literature methods [16].

3.1. Preparation of $[N(PPh_3)_2][Ru_6C(CO)_{16}]$

$Ru_3(CO)_{12}$ (1000 mg) was dissolved in 500 cm^3 of CH_2Cl_2/MeCN (1:1) and the solution cooled to −78°C in a dry ice/acetone bath. Freshly sublimed trimethylamine oxide (240 mg) was dissolved in MeCN (30 cm^3) and added dropwise to the solution over a period of 1 h. After complete addition, the solution was allowed to warm slowly to room temperature during which time it changed colour from orange to orange/yellow to bright lemon yellow indicating the sequential formation of $Ru_3(CO)_{11}NCMe$ and $Ru_3(CO)_{10}(NCMe)_2$. Pyridine (1 cm^3, excess) was added to the solution and its colour changed to orange over a period of 1 h. The solvent was removed under vacuum to yield an orange solid $Ru_3H(CO)_{10}(C_5H_4N)$. The solid was partially redissolved in CH_2Cl_2 and placed in a 180 cm^3 Carius pyrolysis tube and the solvent removed under vacuum whilst rotating the tube to obtain an even coating of the material on the walls. The tube was evacuated to a pressure of 10^{-3} Torr and sealed. The tube was heated at a temperature of 150°C for 48 h yielding a dark brown orange material. The contents of the tube were extracted with acetone containing an excess (1000 mg) of $[N(PPh_3)_2][BF_4]$ and the mixture separated by TLC (acetone/hexane, 1:1). The products were purple/black $[N(PPh_3)_2]_2[Ru_{10}C_2(CO)_{24}]$ (*ca.* 20%) and orange $[N(PPh_3)_2]_2[Ru_6C(CO)_{16}]$ (*ca.* 50%), as identified by IR and mass spectroscopy.

3.2. Preparation of $[N(PPh_3)_2][Ru_6(CO)_{18}]$

$Ru_3(CO)_{12}$ (1000 mg) was refluxed in MeCN (200 cm^2) for 3 h at which point an excess of $[N(PPh_3)_2][BF_4]$ (1000 mg) was added. The solution was cooled and evacuated to near dryness, the mixture was separated by TLC (acetone/hexane 1:1). $[N(PPh_3)_2][Ru_6(CO)_{18}]$ was isolated as the major product (*ca.* 60%) as identified by IR and mass spectroscopy.

3.3. Preparation of $Ru_6C(CO)_{16}Au_2\{Ph_2PCH_2PPh_2\}$ (1)

$[N(PPh_3)_2][Ru_6C(CO)_{16}]$ (100 mg) was dissolved in CH_2Cl_2 and to the stirred solution was added 1.1 equiv. of $Au_2\{Ph_2PCH_2PPh_2\}Cl_2$ and 2.2 equiv. of $TlPF_6$ with stirring overnight. The mixture was filtered

TABLE 6. Atomic coordinates ($\times 10^4$) and equivalent isotropic displacement coefficients ($Å^2 \times 10^3$) for **2**

	x	y	z	U_{eq} [a]
Ru(1)	7583(1)	−225(2)	1985(1)	47(1)
Ru(2)	7555(1)	1706(2)	2743(1)	48(1)
Ru(3)	6266(1)	116(2)	2555(1)	55(1)
Ru(4)	7731(1)	−270(2)	3248(1)	61(1)
Ru(5)	8974(1)	353(2)	2498(1)	57(1)
Au(1)	6603(1)	1567(1)	1677(1)	48(1)
Au(2)	8324(1)	1775(1)	1693(1)	51(1)
C(11)	6832(20)	−1325(22)	1974(14)	84(14)
C(12)	8497(15)	−1129(24)	1902(13)	70(12)
C(13)	7515(15)	−150(17)	1200(12)	55(10)
C(21)	8208(16)	2802(23)	2795(12)	69(12)
C(22)	7562(15)	1452(25)	3562(12)	72(12)
C(23)	6744(17)	2727(22)	2763(10)	59(11)
C(31)	5771(17)	−1072(26)	2840(11)	72(12)
C(32)	5354(20)	412(22)	2033(15)	79(14)
C(33)	5854(17)	938(31)	3111(18)	104(17)
C(41)	8629(19)	−238(25)	3778(15)	83(14)
C(42)	7882(23)	−1683(24)	3052(14)	97(16)
C(43)	7017(21)	−551(23)	3789(14)	85(14)
C(51)	9440(14)	1274(22)	3044(12)	57(10)
C(52)	9641(34)	587(28)	1896(21)	186(30)
C(53)	9553(19)	−785(26)	2849(15)	94(15)
O(11)	6560(16)	−2093(18)	1883(9)	116(12)
O(12)	8853(15)	−1825(17)	1778(11)	119(12)
O(13)	7491(12)	−219(16)	692(9)	88(9)
O(21)	8608(13)	3571(17)	2877(9)	94(10)
O(22)	7569(12)	1744(16)	4046(8)	88(9)
O(23)	6296(13)	3390(17)	2818(10)	98(10)
O(31)	5455(15)	−1812(18)	3049(11)	117(12)
O(32)	4774(13)	504(20)	1790(11)	107(11)
O(33)	5618(16)	1438(21)	3511(13)	142(14)
O(41)	9094(14)	−287(20)	4154(9)	107(11)
O(42)	7997(20)	−2534(18)	2973(11)	151(16)
O(43)	6570(17)	−748(25)	4157(11)	151(16)
O(51)	9744(12)	1840(18)	3367(10)	102(10)
O(52)	10156(14)	790(25)	1620(12)	137(14)
O(53)	9930(14)	−1438(19)	3013(10)	106(11)
P(1)	6452(4)	2453(5)	805(3)	53(3)
P(2)	8257(4)	2714(5)	839(3)	56(3)
C(1)	7331(13)	2418(20)	406(10)	57(7)
C(111)	6212(15)	3855(21)	865(12)	60(7)
C(112)	6234(14)	4306(21)	1400(12)	63(8)
C(113)	6104(16)	5368(23)	1465(14)	77(9)
C(114)	5969(18)	5941(28)	988(15)	93(10)
C(115)	5811(20)	5500(28)	465(16)	107(12)
C(116)	6000(17)	4401(25)	385(14)	90(10)
C(121)	5722(15)	1940(20)	291(11)	59(7)
C(122)	5869(18)	1783(22)	−298(13)	81(9)
C(123)	5282(19)	1368(25)	−688(16)	95(11)
C(124)	4600(20)	1190(25)	−487(15)	92(10)
C(125)	4360(21)	1364(25)	56(15)	100(11)
C(126)	5006(19)	1795(24)	488(15)	95(10)
C(211)	8235(14)	4117(20)	921(11)	56(7)
C(212)	8000(19)	4783(27)	422(15)	101(11)
C(213)	7975(23)	5885(35)	485(20)	139(15)
C(214)	8199(20)	6260(31)	1023(16)	106(12)
C(215)	8309(16)	5676(23)	1473(14)	75(9)
C(216)	8369(16)	4627(23)	1433(13)	76(9)
C(221)	8972(15)	2433(21)	358(11)	59(7)
C(222)	9531(27)	3171(39)	192(21)	162(18)
C(223)	10168(36)	2970(50)	−185(25)	220(27)

TABLE 6 *(continued)*

	x	y	z	U_{eq} [a]
C(224)	10227(25)	1903(33)	−396(18)	130(14)
C(225)	9599(26)	1379(38)	−323(20)	148(17)
C(226)	9028(27)	1584(35)	108(19)	145(16)
O(3)	2239(19)	1769(25)	621(14)	161(12)
O(2)	2483(17)	−299(22)	954(12)	132(10)
C(3)	1734(32)	1235(43)	613(23)	169(20)
C(2)	2796(34)	228(47)	1209(26)	129(25)

[a] Equivalent isotropic U defined as one-third of the trace of the orthogonalized U_{ij} tensor.

and evacuated to near dryness and separated by TLC (CH_2Cl_2/ hexane 90 : 10). The red cluster $Ru_6C(CO)_{16}$-$Au_2\{Ph_2PCH_2PPh_2\}$ was isolated as the main product *ca.* 80–90% yield Anal. Found: C, 27.75; H, 1.20. $C_{42}H_{22}Au_2O_{16}P_2Ru_6$ calcd.: C, 27.18; H, 1.42%.

3.4. Preparation of $Ru_5(CO)_{15}Au_2\{Ph_2PCH_2PPh_2\}$ (2)

$[N(PPh_3)_2][Ru_6(CO)_{18}]$ (100 mg) was dissolved in CH_2Cl_2 and to the stirred solution was added 1.1 equiv. of $Au_2\{Ph_2PCH_2PPh_2\}Cl_2$ and 2.2 equiv. of $TlPF_6$ with stirring overnight. The mixture was filtered and evacuated to near dryness and separated by TLC (CH_2Cl_2/ hexane 90 : 10). The brown/ red cluster $Ru_5(CO)_{15}Au_2\{Ph_2PCH_2PPh_2\}$ was isolated as the main product in *ca.* 50–60% yield Anal. Found: C, 28.18; H, 1.33. $C_{40}H_{22}Au_2O_{15}P_2Ru_5$ calcd.: C, 28.20; H, 1.39%.

3.5. Crystal structure determinations of $Ru_6C(CO)_{16}$-$Au_2\{Ph_2PCH_2$-$PPh\}$ (1) and $Ru_5(CO)_{15}Au_2\{Ph_2$-$PCH_2PPh_2\}$ (2)

Crystal data and data collection parameters for **1** and **2** are summarized in Table 4. The intensity data were recorded at room temperature on a Siemens R3mV four-circle diffractometer using graphite monochromated Mo Kα radiation ($\lambda = 0.71073$ Å). In both cases, the data was corrected for Lorentz-polarization effects and for absorption using a semi-empirical Ψ-scan method. The structures were solved by a combination of direct methods and Fourier difference techniques, and refined by full matrix least-squares analysis (structure **1** on F^2 and structure **2** on F) with all non-hydrogen atoms assigned anisotropic displacement parameters (for **1**) and all non-hydrogen atoms except the phenyl carbon atoms assigned anisotropic displacement parameters (for **2**). The hydrogen atoms for the phenyl and methylene groups in both structures were placed in idealized positions (C–H 0.96 Å) and allowed to ride on the relevant carbon; the isotropic displacement parameters were set at 0.08 Å^2. In the structure of **2**, two solvent molecules of methanol were located and the C and O atoms were refined with individual isotropic displacement parameters. In the final cycles of refinement, a weighting scheme was used which minimized the dependence on F and on sin θ. Refinement continued until convergence was reached. The structures were solved using the SHELXTL-PLUS software package [17] and refined using SHELXTL-PLUS for **2** and SHELXL-92 [18] for **1**. Final atomic coordinates and equivalent isotropic displacement parameters for **1** and **2** are listed in Tables 5 and 6. Full lists of atomic coordinates, bond lengths and angles, and thermal parameters can be obtained from the authors.

Acknowledgements

We are grateful to Johnson Matthey (M.A.B.) and the S.E.R.C. (P.J.B.) for funding and to the European Economic Community for a bursary (M.C.R. de A.).

References

1 I.D. Salter, *Adv. Organomet. Chem., 29* (1989) 249.
2 S.S.D. Brown, I.D. Salter, D.B. Dyson, R.V. Parish, P.A. Bates and M.B. Hursthouse, *J. Chem. Soc., Dalton Trans.*, (1988) 1795.
3 S.S.D. Brown, I.D. Salter and L. Troupet, *J. Chem. Soc., Dalton Trans.*, (1988) 757.
4 A.J. Amoroso, B.F.G. Johnson, J. Lewis, A.D. Massey, P.R. Raithby and W.T. Wong, *J. Organomet. Chem., 440* (1992) 219.
5 A.J. Amoroso, A.J. Edwards, B.F.G. Johnson, J. Lewis, M.R. Al-Mandhary, P.R. Raithby, V.J. Saharan and W.T. Wong, *J. Organomet. Chem., 443* (1993) C11.
6 D.M.P. Mingos and D.J. Wales, *Introduction to Cluster Chemistry*, Prentice Hall, Englewood Cliff, NJ, 1990.
7 C.-M.T. Hayward and J.R. Shapley, *Inorg. Chem., 21* (1982) 3816.
8 B.F.G. Johnson, J. Lewis, S.W. Sankey, K. Wong, M. McPartlin and W.J.H. Nelson, *J. Organomet. Chem., 191* (1980) C3; G.B. Ansell and J.S. Bradley, *Acta Crystallogr., Sect. B, 36* (1980) 726.
9 S.S.D. Brown, I.D. Salter, A.J. Dent, G.F.M. Kitchen, A.G. Orpen, P.A. Bates and M.B. Hursthouse, *J. Chem. Soc., Dalton Trans.*, (1989) 1227.
10 S.R. Bunkhall, H.D. Holden, B.F.G. Johnson, J. Lewis, G.N. Pain, P.R. Raithby and M.J. Taylor, *J. Chem. Soc., Chem. Commun.*, (1984) 25.
11 M.J. Freeman, A.G. Orpen and I.D. Salter, *J. Chem. Soc., Dalton Trans.*, (1987) 379.

12 P.A. Bates, S.S.D. Brown, A.J. Dent, M.B. Hursthouse, G.F.M. Kitchen, A.G. Orpen, I.D. Salter and V. Sik, *J. Chem. Soc., Chem. Commun.*, (1986) 600.
13 D.M.P. Mingos and A.S. May, in: D.F. Shriver, H.D. Kaesz and R.D. Adams (Eds.), *The Chemistry of Metal Cluster Complexes*, VCH, Weinheim, 1990, p. 11.
14 C.M. Hay, B.F.G. Johnson, J. Lewis, R.C.S. McQueen, P.R. Raithby, R.M. Sorrell and M.J. Taylor, *Organometallics, 4* (1985) 202.
15 B.F.G. Johnson, J. Lewis, W.J.H. Nelson, P.R. Raithby and M.D. Vargas, *J. Chem. Soc., Chem. Commun.*, (1983) 608.
16 A. Mantorani and S. Cenini, *Inorg. Synth., 10* (1975) 47.
17 *SHELXTL-PLUS*, *Program Version 4.0*, Siemens Analytical X-Ray Instruments, Madison, WI, 1990.
18 G.M. Sheldrick, *SHELXL-92*, *A Structure Refinement Program*, University of Göttingen, 1992.